

Entanglement Effects in Elastomers: Macroscopic vs Microscopic Properties

Sandra Schlögl

Polymer Competence Center Leoben GmbH, Roseggerstr. 12, Leoben 8700, Austria

Marie-Luise Trutschel and Walter Chassé

Institut für Physik – NMR, Martin-Luther-Universität Halle-Wittenberg, Betty-Heimann-Str. 7, D-06120 Halle, Germany

Gisbert Riess

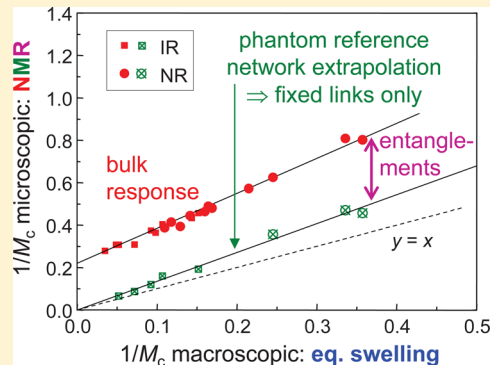
Institute of Chemistry of Polymeric Materials, University of Leoben, Otto Glöckel-Str. 2, Leoben 8700, Austria

Kay Saalwächter*

Institut für Physik – NMR, Martin-Luther-Universität Halle-Wittenberg, Betty-Heimann-Str. 7, D-06120 Halle, Germany

Supporting Information

ABSTRACT: This Perspective highlights how entanglement effects on rubber elasticity can be unveiled by a combination of different macroscopic and microscopic methods, taking advantage of new developments in proton low-field NMR spectroscopy as applied to bulk and swollen rubbers. Specifically, the application of a powerful yet routinely applicable double-quantum method, combined with a back-extrapolation procedure over results measured at different degrees of swelling, allows one to characterize the recently introduced “phantom reference network” state, which only reflects contributions of actual cross-links and topologically trapped entanglements. We further present an assessment of the qualitative yet popular Mooney–Rivlin analysis of mechanical data, where the influence of entanglement contributions on the fitted, purely empirical parameters C_1 and C_2 is reconsidered in the context of different tube models of rubber elasticity. We also review the impact of entanglements on results of equilibrium swelling experiments and address the validity of the common Flory–Rehner approach, where we stress its qualitative nature and the need to use NMR observables for a correct estimation of the relevant volume fractions. We discuss semiquantitative estimations of the cross-link density from these macroscopic experiments with its microscopic determination by NMR on the example of lowly cross-linked synthetic and natural poly(isoprene) rubber prepared by a novel UV-based curing protocol of dried latex based upon thiol–ene chemistry, which in contrast to previously studied thermally peroxide-cured natural rubber contain only small amounts of short-chain defects. We find that the entanglement effects in these samples can best be described by the Heinrich–Straube tube model with positive scaling exponent $\nu > 0.3$ as well as by the slip-link model of Ball et al./Edwards–Vilgis with a slip parameter $\eta > 0.1$. A comparison with literature results demonstrates that these findings are not universal in that the apparent entanglement contribution depends significantly on the sample (in)homogeneity, i.e., of the NMR-determined fraction of inelastic defects and spatial cross-linking inhomogeneities. This means that conclusions on the validity or invalidity of specific tube theories cannot be drawn without careful consideration of the network microstructure.



I. INTRODUCTION

The theoretical foundations of our understanding of entropic rubber elasticity have been laid more than 80 years ago.^{1,2} While these early theories provide a qualitative description of some mechanical properties, e.g., uniaxial stress-strain curves, deviations on the detail level are clearly apparent, in particular for lowly cross-linked systems. The subsequent decades have witnessed the development of a multitude of strain energy functions based upon molecular models and corresponding

stress-strain predictions.^{3–16} The earliest attempts, for example the model of Ronca and Allegra,³ were based upon specific anisotropic constraints to the cross-link fluctuations, which were assumed to be isotropic in the original phantom model.²

Received: December 23, 2013

Revised: April 2, 2014

Published: April 14, 2014

Most modern theories are based upon the tube model of rubber elasticity and all have in common that they assume an additive contribution of chemical cross-links described by one of the classic theories,^{1,2} possibly refined by finite-extensibility terms,^{6,8,13,15} and the entanglement contribution, modeled by slip links^{5,6} or a suitable tube-like constraint^{4,7–12,14,16} to the conformational freedom of all segments rather than just the ends.

With increasing complexity (i.e., number of fitting parameters), fits of simple uniaxial-extension data to such predictions becomes ambiguous,^{7,8,17} stressing the importance of either probing more complex (in particular biaxial) deformation modes^{7,18–22} or, alternatively, the microscopic observation of the structure or the dynamics of individual chains or segments.^{7,8} In this context, neutron scattering techniques^{23,24} have been used to probe the anisotropic stretching of labeled network chains and the anisotropy of the tube-constrained segmental motion, suggesting the validity of a specific tube deformation law. It should be noted that these results have been criticized with regards to the approximations used in the fit of the structure factor and to the contribution of defects.²⁵

Another important and extensively used molecular-scale technique to characterize elastomers is ¹H solid-state NMR, possibly applied on a simple low-field instrument.^{26–40} In particular, the robust double-quantum (DQ or, more generally, multiple-quantum, MQ) technique represents a more quantitative alternative to T_2 relaxometry and has been used extensively to estimate the overall cross-link density and asses the sample homogeneity and defect contents.^{28–30,32–36,38} More recently, it was also used to probe the thermodynamic state³⁷ and the inhomogeneous chain deformation³⁹ in swollen samples as well as to characterize the actual chain stretching in strained samples.⁴⁰ A more indirect ²H NMR spin probe technique as applied to biaxially strained samples was further used to asses the validity of specific network models for the description of local deformation.⁴¹

Here, we highlight how a combination of three different techniques for the characterization of elastomers, i.e., uniaxial stress-strain, equilibrium swelling, and ¹H DQ NMR experiments, thus combining macroscopic and microscopic observables obtained from bulk and swollen samples, can help to reveal the influence of entanglements. This allows for conclusions on the applicability of specific network models.⁷ As a specific example, we present new data measured on latex-based natural and synthetic polyisoprene rubber prepared by a novel UV-based curing protocol.

We discuss the Mooney–Rivlin (MR) method⁴² as the most popular yet purely empirical approach to mechanical data analysis. It is well-known that the MR strain energy function does not provide a consistent description of mechanical data and that the naive interpretation of the fitted C_2 parameter in terms of the entanglement contribution is *a priori* incorrect.^{18,19} However, the literature provides an ample database of fitted apparent MR parameters C_1 and C_2 , and it is a valid question to ask whether this data is of any use. We thus revisit the problem of separating the relative contributions of permanent cross-links and entanglements to C_1 and C_2 when they are fitted over a defined deformation range. It turns out that the predictions of many of the above-mentioned theories differ qualitatively in this aspect, enabling a distinction.

It is noted that the sample preparation (e.g., the use of a specific curing system) has been shown to exert a decisive influence on the MR parameters even in the same base polymer,^{27,43} which stresses the need to use a molecular-scale characterization technique

such as DQ NMR to assess the microstructure.³³ In this latter study, we were able to unambiguously reveal that peroxide-based cross-linking of natural rubber leads to substantial defect contents and pronounced cross-linking inhomogeneities. The specific and complex processes in latex-based rubbers, involving pre-curing, drying, and postcuring, were also revealed with the same technique, demonstrating again substantial differences between sulfur- and peroxide-based curing.³⁴

The most relevant insights arise from the application of DQ NMR to the study of partially swollen rubbers. To this end, we have recently established the “phantom reference network”, which refers to a back-extrapolated NMR observable representative of the unswollen bulk that only reflects contributions from permanent cross-links,³⁹ as reviewed in this Perspective. The observables from all techniques are converted to semi-quantitative measures of the cross-link density, and the linear correlations between them can be used to draw consistent conclusions on the magnitude of entanglement effects.

This Perspective is structured as follows: In the following section, we review what we consider the most established strategies for elastomer characterization by the three mentioned techniques, with a critical discussion of their limitations. The third section is devoted to a discussion of the influence of entanglements in each of the techniques. We put particular emphasis on the predictions of modern theories of entangled rubber elasticity and how these can be tested on the basis of the parameters obtained from the popular Mooney–Rivlin analysis. The fourth section is devoted to a comparative discussion of actual experimental data on a series of lowly cross-linked poly(isoprene) rubbers. We finally conclude on the use of such multimethod studies, combining macroscopic and microscopic insights, in establishing a broader data basis to ultimately obtain a universal picture of entanglement effects in rubbers.

II. REVIEW OF EXPERIMENTS AND ANALYSIS STRATEGIES

In the following, we discuss the different experimental strategies and the associated theoretical background related to an estimation of the most relevant structural parameter of polymer networks, i.e., the average molecular weight between cross-links, M_c , by the different techniques.

A. Equilibrium Swelling Experiments. The most common approach to the analysis of swelling experiments is the Flory–Rehner (FR) theory,⁴⁴ as based upon the separability hypothesis of the free energies of chain stretching and mixing. Taking advantage of comparisons with NMR experiments (see below), we have in recent years addressed many of the practical^{32,36} and theoretical³⁷ problems related to this approach; for a review see ref 45. As the bottom line, we found that FR theory is well applicable in poor and θ solvents, but limitations are expected in good solvents. This is a result of excluded-volume statistics of the chains, which challenges the validity of the treatment of the elastic response. The good news is, however, that the FR equation can still be applied and that the good-solvent effects are phenomenologically accounted for by an (apparently!) concentration-dependent Flory–Huggins interaction parameter χ , as addressed extensively in the literature.^{46–50} Ultimately, one must of course always expect a certain level of systematic error related to the derived absolute values of the obtained molecular weight $M_{c,sw}$.

On the basis of a study of samples with variable effective cross-link functionality f ,³⁶ we found that the FR equation as based upon the phantom model for the elastic response

$$M_{c,sw} = -\frac{\rho_p V_s \phi_{p,el}^{1/3}}{\ln(1 - \phi_p) + \phi_p + \chi \phi_p^2} \frac{f - 2}{f} \quad (1)$$

gives the most consistent representation of the data. This was also stressed much earlier by Cohen and co-workers.⁵¹ Usually, $f = 4$ for elastomers made from long precursor chains. As to the other parameters, ρ_p is the polymer density, V_s the solvent molar volume, $\phi_p = V_p/V$ the polymer volume fraction at swelling equilibrium, and $\phi_{p,el} = \phi_p(1 - \omega_{def,sw})$ the volume fraction of elastically active polymer; i.e., it is corrected for elastically inactive network defects as determined by DQ NMR (see below).

This last issue turns out to be rather relevant, as we find that the fraction of nonload-bearing chains in the swollen state can be rather high, much higher in fact than the amount of extractable sol. Note that the NMR determination of $\omega_{def,sw}$ to be used for $\phi_{p,el}$ in eq 1 must be determined in the swollen state using a perdeuterated solvent. It will be shown below that $\omega_{def,sw}$ can further be substantially bigger than ω_{def} determined in the bulk, in particular in rather lowly cross-linked networks. The defects comprise dangling chains as well as sol. Yet, for rubbers made from long chains, such as the samples addressed below, the sol content is usually rather low.

It should be noted that during swelling experiments it is sometimes mandatory to exclude air and UV light in order to avoid gradual network degradation. This has been demonstrated to be a potentially serious problem for natural rubber swollen in toluene.³² Such adverse effects can be monitored by swelling kinetics studies, as addressed in the Supporting Information.

B. Characterization of Tensile Properties. Rubber materials generally exhibit strongly nonlinear stress-strain behavior, and the elasticity in the lower deformation range can often be described qualitatively by the Mooney–Rivlin (MR) law.⁴² It is again stressed that the MR law must be considered as empirical, as its has no immediate theoretical justification in terms of an entanglement model and since the underlying strain energy function fails qualitatively in the description of mechanical data in more complex (mostly biaxial) deformation modes.^{18,19} However, it represents the most popular approach to simply parametrize the nonlinear tensile behavior. The relevant MR equations for uniaxial extension read

$$\sigma = 2C_1 \left(\lambda - \frac{1}{\lambda^2} \right) + \frac{2C_2}{\lambda} \left(\lambda - \frac{1}{\lambda^2} \right) \quad (2)$$

$$\sigma_{red} = \frac{\sigma}{\lambda - \lambda^{-2}} = 2C_1 + \frac{2C_2}{\lambda} \quad (3)$$

where $\lambda = L/L_0$ is the deformation (stretch ratio) determined by L_0 and L as the initial and final lengths of the sample before and after application of force, respectively. By plotting the reduced Mooney stress (σ_{red}) against the reciprocal $1/\lambda$, a linear relationship, eq 3, is often found or is simply imposed, and the apparent MR constants C_1 and C_2 can be determined by linear regression in a range of small to intermediate deformations, i.e., $1.3 < \lambda < 2.5$ for our data to be discussed below and in many references (see e.g. ref 10).

Sample data are shown in Figure 1 in order to highlight the limitations often posed by actual data and to demonstrate why a two-parameter description based upon a linear fit over a limited data range is practically sufficient. An upper limit (lower limit for $1/\lambda = 0.4$) for the linear fit is chosen to avoid the region of strain hardening due to strain-induced crystallization and finite extensibility. One may of course try to capture these effects

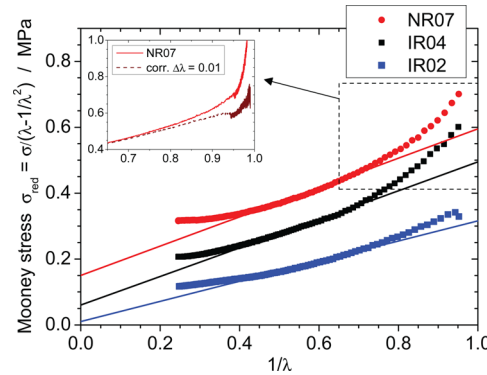


Figure 1. Mooney–Rivlin plot of three poly(isoprene) rubber samples (symbols) showing data up to $\lambda = 0.95$ and linear fits (lines) covering the range of $\lambda = 1.3–2.5$. The inset shows a magnification of the data for sample NR07 (solid line), now including the range up to $\lambda = 1$, and a data set for which λ was adjusted.

with a more complicated model,^{6,8,13,43} yet this comes at the expense of additional uncertainties with regards to its applicability and limitations. A lower limit (upper limit $1/\lambda = 0.77$) is of practical origin and avoids the low- λ region where σ_{red} often shows a strong upturn (in fact, a divergence) due to uncertainties in the determination of λ on many tensile testers. An adjustment by $\Delta\lambda$ can be attempted by fitting the region up to 3% strain to eq 2 using $\lambda - \Delta\lambda$ instead of λ as argument. The inset of Figure 1 demonstrates that the upturn can partially be removed in this way, but uncertainties remain. From the inset, it is however clear that the problem does not significantly affect data below $1/\lambda = 0.8$. While the fitting limits are of course to some degree arbitrary, it is noted that the discussed experimental and theoretical (see below) results hardly change when the fitting limits change within a reasonable range or when e.g. a polynomial fit is used to determine a tangent to the data at $1/\lambda = 0.6$.

For the analysis and comparison of the results to other techniques, it is common practice to take an empirical approach and use the predictions from rubber elasticity theory,^{52,53} again using the relations based upon the phantom model:

$$E = \frac{3\rho_p RT}{M_{c,E}} \frac{f - 2}{f} \quad (4)$$

$$2(C_1 + C_2) = \frac{\rho_p RT}{M_{c,MR}} \frac{f - 2}{f} \quad (5)$$

$$2C_{1/2} = \frac{\rho_p RT}{M_{c,C1/2}} \frac{f - 2}{f} \quad (6)$$

As discussed above in the context of swelling experiments, our previous studies on model elastomers³⁶ suggest that the phantom model is better applicable than the affine model even in bulk rubbers, even though this issue is still a subject of current discussion.⁵⁴ In any way, the affine and phantom predictions differ only in the constant factor $(f - 2)/f$, which only affects the absolute values but not the correlations between them,⁵¹ given constant functionality f . Of course, the phantom model does not explicitly treat entanglements, but it is again common practice to apply one of the classic models to estimate their density from their modulus contribution. In the above equations, we distinguish $M_{c,MR}$ obtained from the $\lambda \rightarrow 1$ limit of the MR analysis, reflected by eq 5, which should be comparable to $M_{c,E}$

from Young's modulus and contain also all entanglement contributions, and $M_{c,Cl}$ as obtained from C_1 only, eq 6, which is often, yet often wrongly, associated with the sole contribution from actual cross-links. These issues will be scrutinized in detail below.

Similar to $\phi_{p,el}$ in swelling experiments (see eq 1), the polymer density $\rho_{p,el} = \rho_p(1 - \omega_{def})$ should possibly also be corrected for a potentially known fraction of sol and elastically inactive defects. Because of the direct proportionality, the correction is of higher relevance here, yet it is less clear how to obtain this information. While Klüppel has suggested an estimation based on the entanglement trapping factor,⁴³ we can here test the more direct assessment by NMR. As discussed below, the NMR-detected apparent defect fraction ω_{def} measured in bulk is often negligible, while $\omega_{def,sw}$ from swollen samples is rather high and varies nontrivially. It is an open issue in how far the topological trapping of long-chain defects, that relax fast only in the swollen state, leads to a slowdown or even arrest of their terminal dynamics and, thus, in how far they contribute to the bulk elasticity.

C. Proton Low-Field Solid-State NMR Spectroscopy.

Proton double-quantum (DQ), or, more generally, multiple-quantum (MQ), NMR experiments have in our hands turned out to be the most robust and quantitative tool for the microscopic (chain-level) analysis of network structure and dynamics.^{29,35} It allows us to obtain a richer, more detailed insight than the closely related technique based upon transverse relaxation (T_2), which was identified to be prone to artifacts if not analyzed properly.⁵⁵ Technically, this is due to the recording of two different (rather than just one) signal functions, which are measured as a function of the pulse sequence duration and analyzed in a combined fashion to obtain (i) the amount of isotropically mobile, thus nonelastic components referred to as defect fraction ω_{def} , which comprises short dangling ends and loop structures, and (ii) the so-called normalized DQ intensity buildup curve. This curve encodes the residual dipolar coupling constant D_{res} (units: rad/s) arising from the nonisotropic orientation fluctuations of actual network chains as well as its potential distribution in an inhomogeneous sample.

The through-space $^1\text{H}-^1\text{H}$ dipole–dipole coupling within monomer units is a weak first-order perturbation of the Larmor frequency and depends on the fixed internuclear distance and on the instantaneous orientation of a given proton pair. This spin interaction is averaged to zero in case of fast isotropic reorientations, but a finite and well-defined average value D_{res} remains for monomers in network chains fluctuating between two fixed ends (cross-links or other topological constraints). In elastomers with chemically simple monomers, D_{res} is an effective value characteristic for all protons in a given monomer and is proportional to the dynamic chain order parameter S

$$D_{res} \propto S = \frac{1}{2}[(3\langle \cos^2(\theta) \rangle - 1)] = \frac{3}{5} \left(\frac{lR}{R_0^2} \right)^2 \quad (7)$$

where $\langle \dots \rangle$ denotes the thermal average over all conformations of a network chain and $[\dots]$ denotes the structural average over all segments in the sample. The angle θ refers to the instantaneous segmental orientation with respect to the end-to-end vector of the given chain. The proportionality factor in eq 7 can be derived on the basis of model considerations.²⁸ A dependence on the state of strain enters via the end-to-end distance R , which may be different from the unperturbed average value R_0 . This is relevant for studies of swollen^{37,56,57} and uniaxially strained samples.⁴⁰

Realizing that in an undeformed sample $R^2 = R_0^2 = Nl^2$, D_{res} can be related to the (apparent) network chain molecular weight

$$M_{c,NMR} = \frac{d_{ref}}{D_{res}/2\pi} \frac{f-2}{f} \quad (8)$$

where for instance $d_{ref,NR} = 617$ Hz kg/mol for natural rubber (NR = 100% *cis*-polyisoprene). The functionality of the cross-links $f = 4$ enters again through application of the phantom model, which was recently shown to provide an improved correlation even in bulk samples.³⁶

Importantly, with our method we can reliably determine from the DQ buildup curve not only the structure-averaged $D_{av} = \langle D_{res} \rangle_{sample} \sim 1/M_{c,NMR}$ described by an averaged version of eq 7 but also its distribution in an inhomogeneous sample. The distribution function can be determined by a previously published, optimized numerical procedure.⁵⁸ The most practical second parameter is the numerically calculated standard deviation σ of the distribution in terms of a dimensionless width parameter σ/D_{av} . In the following, $M_{c,NMR}$ always represents an average value obtained from D_{av} .

III. CONSIDERATIONS OF ENTANGLEMENT EFFECTS

The proposed experimental strategy to be illustrated in the next section relies on extracting information on entanglement effects by comparison of different methods which depend rather differently on these. In the following, we thus address this issue for the case of mechanical, swelling, and NMR experiments, where in the latter, our comparison of samples measured in the bulk and in the swollen state (using an extrapolation procedure) is of particular relevance.

A. Entanglement Effects on Mechanical Properties. For the MR model, it is commonly and uncritically, and likely wrongly, assumed that the constants C_1 and C_2 reflect the contributions of cross-links and entanglements, respectively. This is motivated by the assumption that the topological constraints leading to the entanglement contribution vanish at infinite strain. This is borne out qualitatively by many modern theories of rubber elasticity based upon tube theory,^{4,7,9,12,16} but the λ dependence turns out to be different from $C_2\lambda^{-1}$ when a correct constitutive model is employed. Most of the mentioned tube models rely on specific assumptions on the deformation of the spatial components ($i = \{x, y, z\}$) of the tube diameter

$$d_i = d_0 \lambda_i^{\nu} \quad (9)$$

where affine tube deformation corresponds to $\beta = 1$ and $\nu = 1$. This general form of a tube deformation law has been suggested by Heinrich and Straube (HS) in the context of their mean-field theory, where $0 \leq \beta \leq 1$ describes the influence of (defect-related) constraint release processes and ν is the scaling exponent of actual tube deformation.⁷

For other theories, in particular the molecular stress function model (MSFM) of Wagner^{9,10} and the virtual-chain models of Rubinstein and Panyukov (RP),^{12,16} we find the explicit statement that the entanglement contribution to the modulus, G_e , contributes in equal parts (50–50) to C_1 and C_2 .^{10,12} As we will see, this statement requires some reconsideration.

In general, the nonlinear contributions to the reduced Mooney stress is most often written the form⁴³

$$\sigma_{red} = G_c + G_e \varphi(\lambda) \quad (10)$$

where $\varphi(\lambda) = 1/\lambda$ corresponds to the MR form. Neglecting finite extensibility effects, eq 10 holds for all but one¹⁴ of the cited

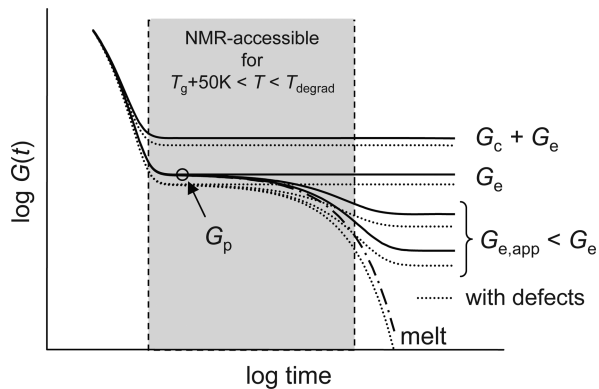


Figure 2. Schematic influence of cross-links, entanglements, and defects on the stress relaxation modulus $G(t)$ of a polymer melt. Since the NMR observable relies on fast segmental motions >100 kHz, it is limited to probing properties reflecting $G(t)$ in the indicated region. Adapted from ref 10.

theoretical treatments based upon molecular (chain) models, but not for possibly improved phenomenological models based upon continuum mechanics. The parameters of these are not readily comparable to results of other methods probing network structure; thus we exclude them in our discussion. From now on, we denote with G_c the contribution of cross-links, which possibly includes topologically trapped entanglements that behave like fixed physical links.^{43,59} G_e reflects apparent entanglement contributions, whose magnitude depends on the particular form of $\varphi(\lambda)$ which may also have an *apparent* λ -independent plateau contribution.

The way in which G_e is reflected in the linear stress relaxation modulus is shown in Figure 2. Wagner¹⁰ argued that the nonlinear response (strain energy function) of a lowly cross-linked elastomer at higher λ is qualitatively indistinguishable from that of a terminally unrelaxed (tube-dominated) polymer melt, where chemical links replace entanglements up to a level where the apparent long-time G_e equals the melt plateau modulus G_p . Such an assumption is at least in partial variance to experimental observations that often show a linear relation and an entanglement-related intercept when the elasticity modulus is plotted vs the cross-linker content.^{38,60}

However, relaxation processes of a long cross-linked but entanglement-dominated chain within the tube are certainly possible,⁶¹ such that the relaxed modulus and depends non-trivially on the cross-linker content. Trapped entanglements acting as physical cross-links, and possibly following the deformation law of a permanently cross-linked rubber,^{43,59,62} are another issue. Thus, the relaxed modulus $G_{e,app}$ cannot *a priori* be expected to be proportional to the actual cross-link density, and it may well be lower than G_e . Finally in this context, it is also useful to bear in mind that fast-relaxing defects (short loops, dangling ends) effectively dilute the system and reduce the long-time modulus over a large time range (dotted lines in Figure 2).

Turning back to tube-model predictions of $\varphi(\lambda)$, Figure 3 shows a representation of the entanglement-only contribution ($G_c = 0$) normalized to $G_e = 1$ to the Mooney stress for the most relevant of the mentioned theories: MSFM,^{9,10} RP1997 simple virtual chain scaling model,¹² RP2002 extended slip-tube model,¹⁶ and the HS mean-field tube model.⁷ For the latter

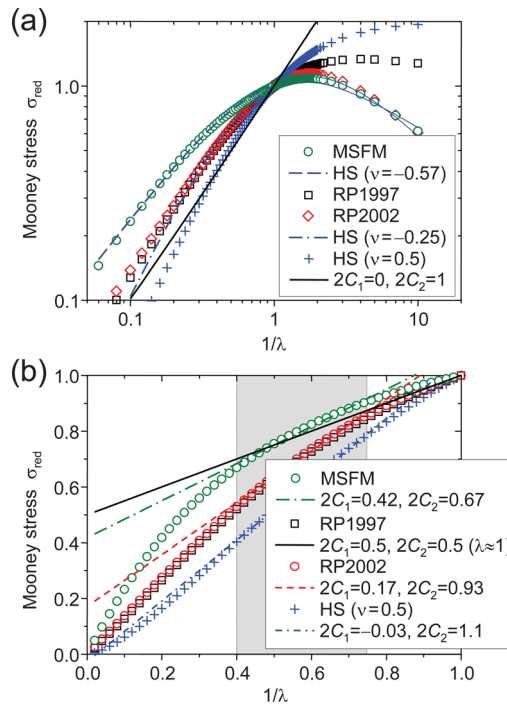


Figure 3. Predictions of the different tube theories for the reduced Mooney stress σ_{red} as a function of inverse strain for the purely entangled case ($G_c = 0, G_e = 1$) (a) on a log–log scale and (b) on a linear scale for the elongation range. Lines with indicated $C_{1,2}$ values are linear MR predictions or fits. The fitting range in (b) was $0.4 \dots 1/\lambda \dots 0.75$, except for the fit to the RP1997 data (solid line), which represents the slope at $1/\lambda = 1$. MSFM: molecular stress function model;^{9,10} RP: Rubinstein–Panyukov models;^{12,16} HS: Heinrich–Straube model⁷ with scaling parameter ν .

$$\varphi(\lambda) = \frac{1}{b} \left(\frac{\lambda^b - \lambda^{-2b}}{\lambda^2 - \lambda^{-1}} \right) \quad (11)$$

where $b = \nu\beta$. In Figure 3a, it is seen that only the MSFM, RP2002, and HS ($\nu < 0.5, \beta = 1$) models can account for the (experimentally well substantiated) maximum of σ_{red} at slight compression ($\lambda \approx 0.56$).

An interesting observation is that the HS model can, almost perfectly, reproduce the predictions of all other tube models by variation of the tube scaling exponent ν . We are aware of only one treatment that mentioned the close relation of the HS and RP models¹⁴ and stress its heuristic use. Specifically, $\nu < 0$ corresponds to an *oblate* tube constraint, and $\nu = -1/4$ has been claimed to hold for highly cross-linked networks.⁷ A value of $\nu = 1/2$ was in turn attributed to entanglement-dominated rubbers. The MSFM also assumes entanglement-dominated systems,⁹ assuming an *isotropic* dilation $\sim \lambda^{1/2}$ of the tube upon uniaxial stretching, which in the anisotropic HS model occurs for the *transverse* component when $\nu < 0$. This may explain the fit with the larger $\nu \approx -0.57$ exponent. Interestingly, the RP2002 model corresponds to $\nu = -1/4$ even though it explicitly assumes a $\lambda^{1/2}$ scaling of the tube diameter component parallel to the strain. The difference is obviously explained by the different—obviously inverse—way in which the tube constraint is implemented in the different models (virtual chain length versus mean-field harmonic potential).

We thus conclude that the HS tube model represents the currently most versatile tube-based approach, as one can in principle use eqs 9–11 in combination with experimental data to

draw conclusions on the value of ν when it is taken as a free parameter (of course setting $\beta = 1$). It is noted that the early theory of Ronca and Allegra, assuming a specific form of restrictions to junction fluctuations rather than a tube constraint,³ and the tube model of Marrucci⁴ also predict the experimental maximum in σ_{red} , however not at $\lambda \approx 0.56$ but at $\lambda = 1$. Both models predict a quicker decay of σ_{red} with $1/\lambda$ in the compression range than the other models. In elongation, the Marrucci model is similar (but not identical) to the HS model with $\nu = 1/2$.¹¹ Further, the Ronca–Allegra model predicts a constant ratio of C_1/C_2 (as it does not consider an independence of cross-link and entanglement effects) and a rather strong, nonlinear, and decisively sigmoidal decay of σ_{red} with $1/\lambda$ in the elongation range. Both latter models are thus not in good accord with experimental data and can safely be neglected.

Figure 3b is of relevance for MR analyses, as it shows that MR fits in the elongation range, when suitably (and experimentally reasonably, see above) constrained to intermediate $1/\lambda$ values, will show finite contributions of G_e to the apparent $2C_1$ even in a purely entangled system. The 50–50 statement of Wagner¹⁰ refers to exactly this situation, while the 50–50 statement in RP1997¹² actually refers to the slope around $\lambda \approx 1$. Analyzing the RP predictions, both of which coincide in the elongation range, in the intermediate λ range yields $2C_1 \approx 0.2G_e$ and $2C_2 \approx 0.9G_e$ (not conserving the sum!).

Notably, the HS model with values of ν larger than around 0.3 is for simple linear stress–strain observations practically indistinguishable from the MR form (in particular, considering the uncertainties discussed in the context of Figure 1). The MR form is exactly recovered for $\nu = 1$ (affine tube deformation). Thus, for this range, $2C_1 \approx 0$ and $2C_2 \approx G_e$, in agreement with common operational interpretation of the C_2 term.

Another relevant entanglement model is the slip-link theory of Ball, Doi, Edwards, and Warner,⁵ for which a tube-based treatment of finite-extensibility effects was later developed by Edwards and Vilgis (EV).⁶ The best approximation for $\varphi(\lambda)$ in the limit of infinite extensibility ($\alpha = \lambda_{\max}^{-1} \rightarrow 0$) is⁶

$$\varphi(\lambda) = \frac{\lambda}{D\theta^2} - \frac{1}{D(\lambda + \eta)^2} + \frac{\eta\lambda}{\theta(\lambda + \eta)} \quad (12)$$

where $D = \lambda - \lambda^{-2}$ and $\theta = 1 + \eta\lambda^2$ (correcting a typo in the first term of eq 12 in the original publication). The parameter characterizing the “slippage” of the entanglements is η . The EV model has been tested in uniaxial extension using MR fits^{63,64} and also in biaxial deformation.²⁰ The latter work compared it to other molecular theories, among them the HR and RP models, and identified the EV model with $\eta = 0.08$ as the best-fitting tube-based model for the special case of long-chain end-linked PDMS model networks.

Neglecting finite extensibility, the data plotted in Figure 4 show another Mooney representation of the entanglement-only case, now for the EV model in the range of realistic slip parameters η . It is seen that the linear MR fits to the intermediate λ range produce $2C_1 \approx 0$ only in the range $\eta > 0.1$ (significant slip). Thus, in this range, $2C_2 \propto G_e$ with a proportionality factor that decreases with increasing slip, as intuitively expected, since the entanglements are less and less effective. In the range $\eta < 0.1$ we find increasingly large contributions of G_e to the apparent $2C_1$ with roughly conserved sum, approaching the limit $2C_1 \approx G_e$ for vanishing slip, when entanglements behave as phantom-type cross-links.⁶ The solid line shows for one example that finite

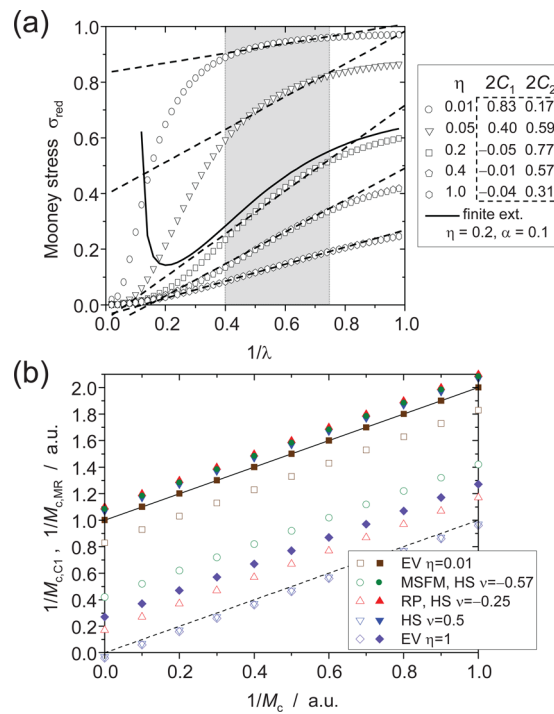


Figure 4. (a) Predictions of the slip-link theory of Ball et al.⁵ and Edwards–Vilgis⁶ for the reduced Mooney stress σ_{red} as a function of inverse strain for the purely entangled case ($G_c = 0, G_e = 1$) on a linear scale for the elongation range, varying the slip parameter η . The dashed lines with indicated $C_{1,2}$ values are fits over the $0.4 \dots 1/\lambda \dots 0.75$ range, and the solid line includes finite extensibility effects⁶ with $\lambda_{\max} = \alpha^{-1} = 10$ for the $\eta = 0.2$ case. (b) Apparent network chain densities derived from C_1 and $C_1 + C_2$ values (open and solid symbols, respectively) of MR fits to different tube model predictions as a function of known cross-linked chain density $1/M_c$ for a fixed $1/M_e = 1$. The dashed and solid lines are the respective expectations when C_2 is assigned to the full $1/M_e$ contribution.

extensibility produces an upturn as well as a slight ($\sim 10\%$) offset contribution to the apparent $2C_1$, which is true for any value of η .

Finally, we mention the “double tube model” of Mergell and Everaers,¹⁴ which has been shown to fit data from computer simulations very well.⁶⁵ It assumes a homogeneous confining potential determined by a tube parameter that combines the effect of both entanglements and actual cross-links. This model is constructed as an interpolation between the RP model and the phantom prediction for permanent cross-links, and it thus covers roughly the same range of apparent $C_{1,2}$ values as the EV model for $\eta \leq 0.1$. A distinction between the models is certainly only possible on the basis of multiaxial mechanical experiments, for which the corresponding equations have not yet been derived.²⁰

Summarizing, one can state that all of the discussed entanglement theories predict that both apparent MR fit parameters $C_{1,2}$ contain entanglement contributions to a variable degree, which for the HS and EV models is parametrized by the tube scaling exponent ν and the slippage parameter η , respectively. For approximately $\nu > 0.3$ and $\eta > 0.1$, respectively, the original MR assumption of $2C_1 \approx 0$ and $2C_2 \propto G_e$ holds apparently. A comparison with experimental data from other methods for a series of networks with variable cross-link density can thus help to draw conclusions validity of a specific theories and on the meaning of the two apparent parameters. This is demonstrated by the data in Figure 4b, which show apparent network chain densities from MR fits to the different model

predictions for a fixed $1/M_e$ as a function of a known $1/M_c$ value, which, as demonstrated below, can be taken from swelling or NMR experiments. First, we note that all models except the EV model for slippage parameters >0.1 predict that $1/M_{c,\text{MR}}$ calculated from the apparent $C_1 + C_2$ (eq 5) is a rather good measure of the overall constraint density, despite the crude linear approximation over a limited $1/\lambda$ range. Second, relevant and meaningful differences among the models arise for $1/M_{c,C1}$ calculated from the apparent C_1 only (eq 6). Only the HS model with $\nu > 0.3$ or the EV model with $\eta > 0.1$ yield dependencies with near-zero intercept, indicative of a vanishing entanglement contribution to the apparent C_1 . All other theories lead to higher intercepts, and its ratio to the intercept of $1/M_{c,\text{MR}}$ can be used to constrain the range of valid theories. It is finally noted that model uncertainties will of course lead to nonunity slopes in such a plot, yet the ratio of the intercepts remains to be a valid measure.

B. Entanglement Effects on Equilibrium Swelling. The interplay of entanglements with the results from equilibrium swelling experiments appears to be relatively clear. A relevant experimental observation is that the apparent C_2 vanishes in the limit of highly swollen samples,¹⁰ i.e., for $\phi_p < 0.25$, and Edwards and Vilgis have given a molecular interpretation of this finding in terms of their slip-link theory.⁸ It can thus be concluded that swelling experiments should reflect the cross-link contribution, possibly also containing the trapped-entanglement fraction, here jointly denoted as G_c .

It should however be noted that biaxial strain experiments on swollen rubber have shown that an apparently vanishing C_2 does not necessarily imply that the classical neo-Hookean model is now valid for the swollen state.^{21,22} Only a more complicated, phenomenological strain energy function could provide the basis for a good fit in these works. This could imply that trapped entanglements do not deform in a simple way, but further work is certainly necessary to elucidate the molecular underpinnings of this finding.

C. Entanglement Effects on NMR Observables. For NMR it is important to consider the dynamic nature of the actual experimental observable, i.e., the residual dipolar coupling constant D_{res} . It reflects fast conformational averaging on time scales up to the 10–100 μs range. Figure 2 shows that this requirement limits NMR observations to the region around G_p . In this range, the NMR measure was in many publications^{28,32,33,35,36,38} shown to exhibit an almost perfect linear relationship to moduli as well as equilibrium swelling results. In addition, it provides a reliable measure of the nonelastic defect fraction for which $D_{\text{res}} = 0$.

For an assessment of the entanglement contribution in this range, assuming additivity in D_{res} or related quantities, earlier approaches were based upon a subtraction of an effective entanglement effect by simply subtracting the result measured on an un-cross-linked melt at the same temperature.²⁷ This approach is identified as ambiguous in the light of Figure 2, since the melt result is a strong function of temperature while the network results is not.⁶⁶ Rather, assuming a constant entanglement density and additivity of entangled and cross-linked chain densities, we can write $D_{\text{res}} \sim 1/M_{c,\text{NMR}} + 1/M_e$, with M_e as the entanglement molecular weight. Exploiting the stably observed linear relationship of D_{res} with other, macroscopic measures of cross-link density (hopefully $\sim 1/M_c$), an extrapolation over a range of different samples consistently identifies an intercept value, i.e., a finite $D_{\text{res},e} \sim 1/M_e$ in the limit of an un-cross-linked melt.^{28,32,33,38} Truly systematic investigations of

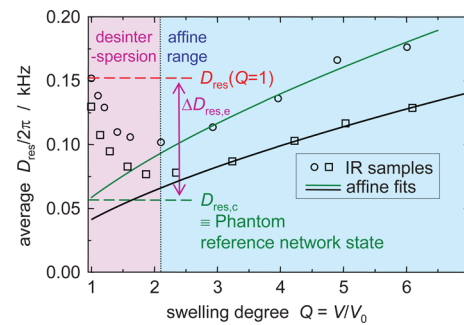


Figure 5. Influence of swelling on the NMR observable D_{res} for two different samples, showing the extrapolation procedure over the affine deformation range to extract the $D_{\text{res},c}$ characterizing the phantom reference network (PRN) state, where only chemical cross-links and topologically trapped entanglements contribute. Data replotted from ref 39.

$D_{\text{res},e}$ obtained by extrapolation vs different other cross-linking measures are as yet rare,^{32,38} and we shall address this issue below.

Note that in vulcanized samples the density of (trapped) entanglements may itself depend on the cross-link density, posing a possible ambiguity. A recent theoretical study has even suggested that toward lower cross-link densities ($G_{c,\text{app}} < G_p$ in Figure 2) the linear decay of the NMR-detected D_{res} toward a finite value ($1/M_e$) should change into a square-root behavior $\sim 1/(M_e M_c)^{1/2}$ in the very high temperature limit, ultimately approaching zero.⁶¹ This argument is based upon the orientational averaging behavior of the network chain within the tube arising from the dominating entanglement constraints. The resulting decay of $D_{\text{res}} \sim 1/M_{c,\text{NMR}}$ toward zero is, however, generally not found in experiments since the time scale of large-scale chain motions within the tube is much longer than the NMR experimental time scale at relevant temperatures below sample decomposition, thus preserving the linear decay toward $1/M_{c,\text{NMR}} \sim 1/M_e$. This is highlighted by the shaded gray region in Figure 2.

NMR studies on swollen samples can also provide valuable insights into entanglement effects,^{26,31,39,67} as they can be expected to be removed in the limit of low volume fractions in much the same way as in equilibrium swelling experiments. Qualitatively (see Figure 5), one often (but not always) observes an initial decay of the NMR observable upon swelling^{26,31,39,67} measured by the volume degree of swelling $Q = V/V_0$. Operationally, one may just evaluate the pure cross-link contribution $D_{\text{res},c}$ from the minimum, where the topological unfolding ("desinterspersion" of entanglements) may be assumed to be complete.^{26,31,67}

We recently refined this qualitative approach, taking into account the R dependence of D_{res} in eq 7.³⁹ While the early "desinterspersion" stage is not universal and a strong function of preparation conditions, we consistently for many different rubber types found perfectly affine behavior ($R \sim Q^{1/3} \Rightarrow D_{\text{res}} \sim Q^{2/3}$) beyond the minimum. A back-extrapolation yields what we have termed the "phantom reference network" state, with $D_{\text{res},c}$ reflecting the bulk contribution from chemical and fixed physical cross-links. Our previous work has indicated an almost perfect intercept-free proportionality with the equilibrium swelling result.³⁹ This finding, in combination with correlations of $D_{\text{res},c}$ with apparent MR constants C_1 and C_2 will be taken up and scrutinized below.

IV. SAMPLE APPLICATION TO LOWLY CROSS-LINKED POLY(ISOPRENE) RUBBERS

We now turn to a demonstration of the principles explained above, discussing and comparing experimental results obtained from a series of natural and synthetic poly(isoprene) rubber (NR and IR, respectively) prepared by a novel UV-based curing protocol of dried latex based upon thiol–ene chemistry.^{68,69} Such samples, in contrast to previously studied thermally peroxide-cured NR,³³ contain relatively small amounts of short-chain defects. In total, we have prepared and investigated 12 NR samples and 10 IR samples, which are simply numbered according to their increasing average cross-link density. Details on the preparation and characterization of the samples can be found in the Supporting Information.

Of particular importance for the discussion are the reported literature values for the entanglement molecular weights $M_{c,\text{rheo}}$ estimated from melt rheology, which are 3.9 and 6.4 kg/mol for NR and IR, respectively,^{70,71} as explained by the different microstructures. Literature values in fact vary, and we note that a higher value of 6.1 kg/mol is calculated from the entanglement parameters for NR published in earlier work of Ferry and co-workers.⁷²

A. Microstructural Characterization by NMR. Potential inhomogeneities of the cross-linked rubber matrix are assessed by the distribution analysis of residual couplings, as shown in Figure 6a. The caption also indicates average values and the normalized distribution widths, σ/D_{av} , for selected samples. A comparison with previous results^{33,34} reveals that the values are

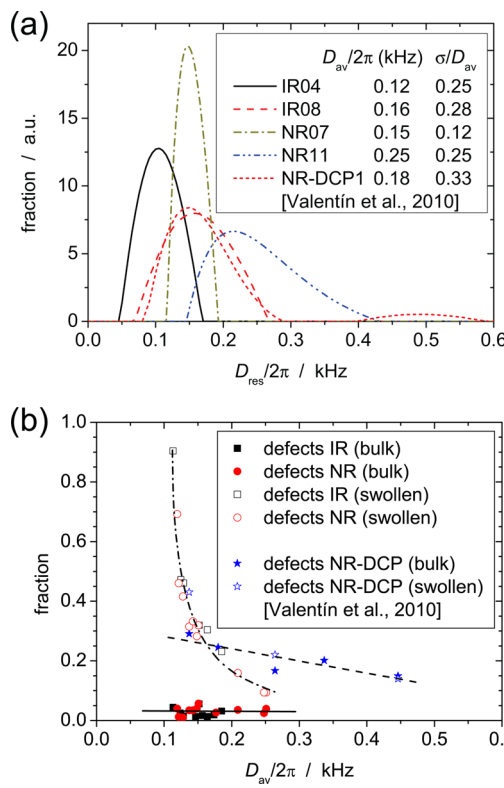


Figure 6. Results of the low-field NMR characterization. (a) Distributions of residual dipole–dipole couplings reflecting cross-linking inhomogeneities and (b) apparent, nonelastic defect fractions as compared to previous results³³ obtained on conventionally, peroxide-cured NR using dicumyl peroxide (DCP). Plot (b) also shows the high defect fractions determined on swollen samples.

in-between the limiting cases of the usually very homogeneous sulfur-based vulcanization schemes ($\sigma/D_{\text{av}} < 0.2$ typically) and radical-based cross-linking using peroxides ($\sigma/D_{\text{av}} > 0.3$). The distributions do not show the second component that is consistently found for the latter case using DCP,³³ where we identified regions of rather high cross-link density, possibly arising from radical chain reactions, but are similarly broad.

The apparent content of elastically inactive defects determined in bulk and in the swollen state is shown in Figure 6b and reveals a striking difference to previous results for DCP-cross-linked NR. The bulk results, being overall very similar to latex-based NR cross-linked with hydroperoxides,³⁴ indicate a low defect fraction in the 5% range. According to Figure 2, this should relate to quickly relaxing low molecular weight defects such as short loops and dangling ends. In contrast, DCP-based NR usually exhibits defects in the >20% range due to excessive chain-scission reactions,³³ which are obviously avoided in the novel preparation scheme.

The situation changes dramatically for the swollen state, where entanglement constraints are removed. Samples not too far above the percolation threshold now reveal around 90% nonelastic chains, which decreases quickly with increasing cross-linking to a level below 30% for most samples. This observation is less dependent on the specific cross-linking reaction and has also been made for sulfur-cross-linked NR^{32,33} as well as different kinds of poly(dimethylsiloxane) rubbers.³⁶ Such high actual defect contents were shown to be in agreement with estimations from Miller–Macosko network theory.^{36,73} Note that the extractable sol content is below 10% on average for the investigated samples, as expected for rubbers based upon long precursor chains.

Importantly, the defect content does not increase much upon swelling in DCP-cross-linked samples,³² which can be explained by the predominance of shorter chain fragments. Without such adverse reactions, as is the case for the given sample series, the defect fraction is composed of long precursor chains that are highly entangled in the bulk. As they are slightly branched, they may exhibit excessively (if not immeasurably) long relaxation times. It is thus a nontrivial and open question to which extent these defects contribute to the bulk mechanical properties.

B. Correlations of Macroscopic Properties. This section part focuses on the correlations of apparent cross-linking parameters as derived from the different methods. Specifically, we address the network chain densities $1/M_c$, which equal twice the density of cross-links in four-functional networks. Since all estimations are based upon specific models and rely on different approximations, we cannot expect perfectly matching values, but we can check whether unique monotonic (in fact, linear) relationships exist. In particular for NMR, where the residual dipolar coupling is an effective monomer-based measure of orientation fluctuation, a number of assumptions must be made, which renders the $1/M_{c,\text{NMR}}$ values uncertain to at least 50%.^{27,28,36,66} However, also the swelling results, in particular when a good solvent is used, are subject to—often neglected—model dependencies that can impose systematic errors of the same order of magnitude.^{32,37}

We first turn to correlations between $1/M_c$ values derived from macroscopic properties, i.e., moduli and swelling results. Figure 7 presents such a correlation based upon the E modulus. We observe significant scatter, which is attributed to the uncertainties of the initial-slope estimation in our tensile tester. Nevertheless, we find an approximately linear correlation with an intercept, indicating additional entanglement effects on E . The plot also

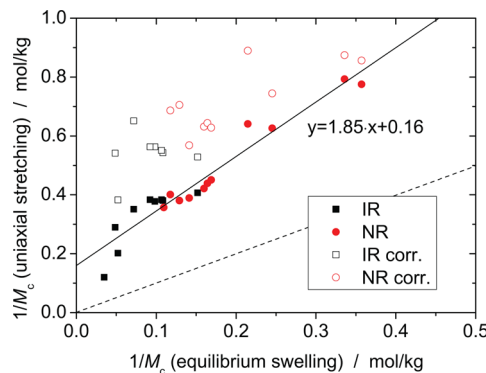


Figure 7. Correlation of the network chain densities calculated from Young's modulus with the analogous quantity derived from equilibrium swelling experiments. The solid line is a linear fit with indicated parameters, and the dashed line has a slope of unity. The open symbols represent values corrected for the defect fraction determined by NMR in the swollen state.

shows the result of an attempt to correct the rubber density for the significant defect fraction found by NMR for swollen samples, using $\rho_{p,\text{el}} = \rho_p(1 - \omega_{\text{def}})$ for the polymer density in eq 4. The scatter increases substantially, and the apparent cross-link densities reach rather large values.

Figure 8a shows corresponding data, now using the (regarding the better data quality more reliable) results from the MR analyses. In particular, the cross-link density derived from $C_1 + C_2$ should be directly comparable to the value derived from E , and we indeed observe a well-defined linear relationship with the swelling results, showing a more reliable intercept, however with a somewhat lower slope. This is not unexpected, as the MR analysis focuses on an intermediate strain range where the Mooney stress may not be linear in $1/\lambda$. As explained in the context of Figures 1 and 3b, such nonlinearities may well be hidden in actual data, leading only to systematic shifts between the two (apparent) parameters C_1 and C_2 . Notably, the C_1 -only data have a zero intercept within the experimental accuracy, suggesting that C_1 indeed reflects the same information as the swelling results, i.e., chemical cross-links plus a fixed-constraint contribution commonly associated with trapped entanglements. This is a common observation that has also been made for sulfur-vulcanized NR.^{38,74} Thus, in the limit of small cross-link densities, entanglements appear to not contribute to C_1 .

Data including the defect correction for the mechanical data, again using $\rho_{p,\text{el}} = \rho_p(1 - \omega_{\text{def}})$ in eqs 5 and 6 as based upon NMR on swollen samples, are shown in Figure 8b. The quality of the correlation now appears better, but in particular for the C_1 -based measure this is deceptive because the large correction for low cross-link densities has a weak effect on the anyways small values. It is thus instructive to focus on the C_2 contribution plotted in Figure 8c, which also includes expected values based on the known entanglement molecular weight of the used polymers. The results without defect correction (solid symbols) imply an on average small difference between NR and IR samples, suggesting that the higher literature value of $M_e \approx 6.1 \text{ kg/mol}$ ⁷² for the former is more reliable. This of course holds only if C_2 does turn out to provide a good measure of G_e .

However, the effect of the defect correction to the mechanical data is rather dramatic, and unrealistically high values result. While $M_{e,\text{app}}$ may well be reduced (its inverse increased) at higher

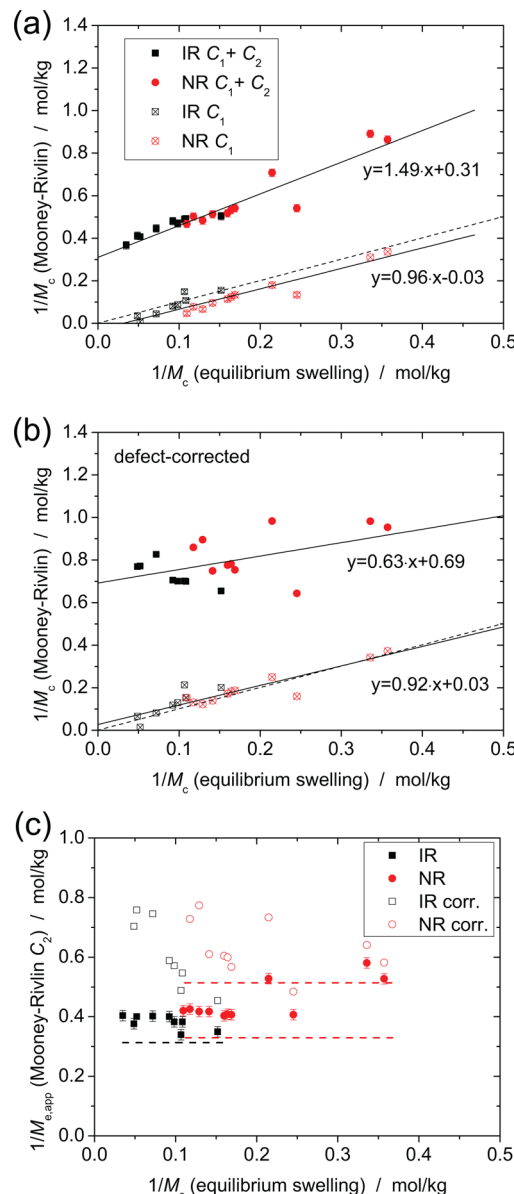


Figure 8. Correlation of the network chain densities calculated from the MR parameters with the analogous quantity derived from equilibrium swelling experiments. (a) Total effective network chain density (from $C_1 + C_2$) and high-strain contribution (from C_1) reflecting mainly chemical cross-links, (b) same as (a) but with NMR-based defect correction, and (c) the apparent entanglement-associated contribution (from C_2). The solid line in (a) is a linear fit with indicated parameters, and the dashed line in (c) has a slope of unity. The dashed lines in (c) indicate the $2/M_{e,\text{rheo}}$ where for NR two different literature values are reported.^{70–72} The factor of 2 accounts for the use of the phantom model that is not implied in the definition of $M_{e,\text{rheo}}$.

cross-linking, there is no reason that $1/M_{e,\text{app}}$ from the melt plateau modulus should be much exceeded in the limit of low cross-link densities. From this, we conclude that the defects, that are unambiguously identified by NMR in the swollen state (and should be used to correct equilibrium swelling analyses), are mechanically active in the bulk; i.e., they do not relax on the time scale of our mechanical testing. This raises the important question whether they would relax on a much longer time scale or are effectively trapped, but an in-depth investigation of this issue is beyond the scope of the present work. For the present

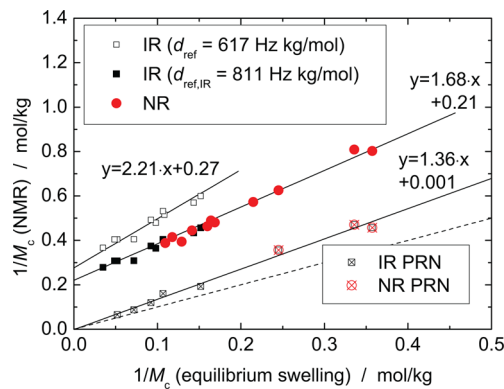


Figure 9. Network chain densities from NMR as compared to swelling results. The solid lines are linear fits with indicated parameters, and the dashed lines have a slope of unity. The crossed symbols denote the NMR values obtained by extrapolation from experiments on swollen samples, i.e., the phantom reference network (PRN) state.

purpose, we therefore focus on the mechanical results without this defect correction.

A relevant conclusion, to be taken up below, is the somewhat steeper slope observed for the $C_1 + C_2$ based measure in Figure 8a. In other words, C_2 increases somewhat with increasing cross-linking, as is also apparent from Figure 8c. Considering the chemical differences between NR and IR, and the fact that the NR samples cover the higher cross-linking range, we can at least say that C_2 does not decrease significantly, which allows for conclusions on the appropriate elasticity model.

C. Correlation of Microscopic and Macroscopic Properties. NMR results are compared with swelling results in Figure 9. Before we turn to the comparison of the different correlations with bulk and PRN results, we address the different behavior of the IR samples shown as open squares. As compared to the NR results (solid circles), the slope is steeper. We attribute this to the microstructural differences. It is known that the NMR quantity D_{res} depends on the specific dynamics within and beyond a monomer, as a result of different conformational statistics, effective chain stiffness, etc.⁷⁵ It is thus not surprising that the model-dependent reference coupling for NR, $d_{\text{ref},\text{NR}} = 617 \text{ Hz kg/mol}$ ²⁸ must be modified for IR. To achieve this, both data sets were simultaneously fitted to a linear relationship, allowing only for a scaled reference value for the IR data. In this way, we obtained a reference coupling $d_{\text{ref},\text{IR}} = 811 \text{ Hz kg/mol}$. Using this new value in the calculation of $1/M_c^{\text{NMR}}$, we obtain the solid squares, which perfectly match the NR results. The following discussions always refer to values for IR obtained in this way.

As to the bulk NMR observable, we again and in analogy the $C_1 + C_2$ based mechanical observable recognize an almost perfect linear correlation with an intercept attributable to entanglement effects. In contrast, the PRN values (taken on fewer samples due to the high effort involved), now in perfect analogy to the C_1 -only mechanical data, follow a linear relation with no intercept. This nicely proves the concept that the PRN indeed characterizes the fixed-cross-link contribution and that C_1 represents a good measure of it. A fortuitous cancellation of errors appears unlikely, considering that all three methods are in qualitative agreement. Also in perfect analogy to Figure 8a, the slope is somewhat steeper for the former, indicating that the entanglement effect reflected in the bulk NMR measure also increases with

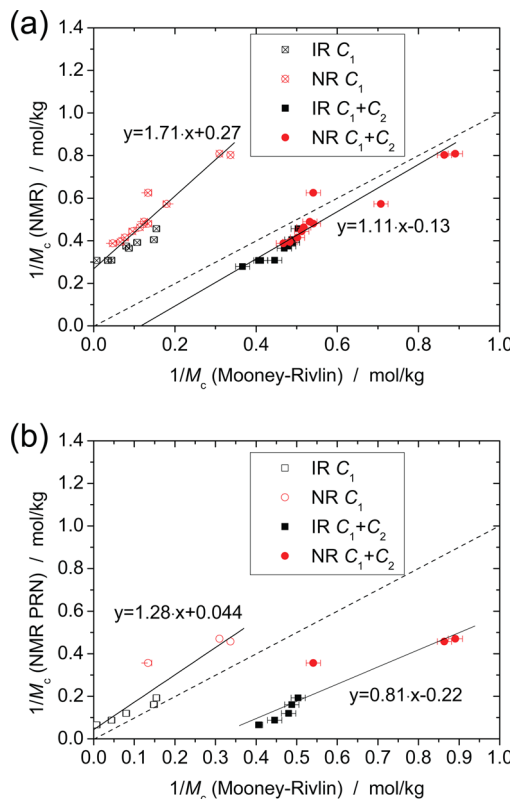


Figure 10. Network chain densities from NMR (a) measured in bulk and (b) obtained by extrapolation over experiments on swollen samples (PRN) as compared to MR results. The solid lines are linear fits with indicated parameters, and the dashed lines have a slope of unity.

cross-linking. Note that the present correlation does not suffer from ambiguities related to a possible correction of the rubber density; rather, the NMR measure characterizes the total elastically active fraction in its associated time range (see Figure 2). Thus, there is a proportionality between the short-time entanglement contribution measured by NMR and the $1/M_{\text{e,app}}$ reflected in the C_2 contribution.

Finally, Figure 10 supplies another set of correlations of the NMR results with the MR results. The two graphs show on the y-axis (a) the bulk NMR measure and (b) the PRN result. The correlations are more noisy, mainly due to the limited accuracy of the mechanical data, but the trends are the expected ones and confirm the observations and conclusions so far: The bulk NMR measure and the PRN limit correlate linearly with closer to zero intercept with the $C_1 + C_2$ and C_1 -only measures, respectively, and again, the increasing C_2 contribution leads to the now flatter slopes of the NMR data versus the $C_1 + C_2$ measure along the x-axis.

D. Discussion of Elasticity Models and Comparison with Previous Results. From the correlations discussed above, we could consistently conclude that (i) fixed-constraint contributions (chemical cross-links plus trapped entanglements) to the swelling-derived $1/M_c$, to the C_1 -based MR measure, and to the extrapolated PRN value from NMR are of identical relative magnitude, and (ii) the entanglement contributions to the mechanical and NMR properties, both as compared to the swelling results, are consistently larger than the fixed-constraint contributions and are increasing slightly with cross-linking. The latter conclusion can be backed up by a final correlation plot comparing two completely independent (in the case of C_2 of course

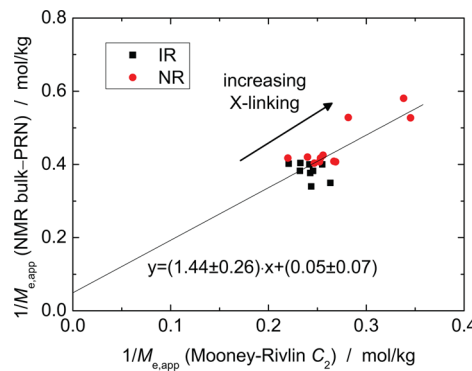


Figure 11. Comparison of the independent microscopic and macroscopic measures of the entanglement contribution from NMR (difference between bulk and PRN) and MR C_2 , respectively. Linearly interpolated PRN values were used for the samples for which an experimental value was not available. The correlation coefficient R for the linear regression is 0.79.

potential) measures of the full entanglement contribution, i.e., the microscopically determined difference between the bulk and PRN NMR values and the MR C_2 -based value, as plotted in Figure 11. The data of course scatter, yet a linear regression demonstrates with good confidence a proportionality with zero intercept. Higher $1/M_{e,app}$ values are found for more highly cross-linked systems.

First of all, higher $1/M_{e,app}$ for higher cross-link densities are in principle expected, as the tube diameter can be expected to decrease, as the chains are increasingly constrained by other chains with decreased cross-link separations. Such a trend, however, is only visible if it is not accompanied by a nontrivial change of the deformation law. We remind that the $C_{1,2}$ values are apparent quantities (see Figures 3b and 4). Negative apparent tube scaling exponents $\nu < -1/4$ of the HS model (oblate tube constraint) as well as small slippage parameters $\eta < 0.1$ of the EV model, which were reported to be valid for highly cross-linked systems,^{7,8} can actually be excluded, as in such cases, the apparent C_1 would exhibit a non-zero intercept when plotted against an objective measure of the fixed-constraint contribution, as safely represented by the swelling results (Figure 4b). Moreover, if the HS exponent changed toward negative values upon moving toward higher cross-link densities, one would expect the apparent C_2 to decrease, contrary to the observation.

Therefore, we conclude that the given sample series is well described by the HS model with a positive tube scaling exponent above around 0.3 or the EV model with a slippage parameter above 0.1, as in this range the apparent entanglement contribution to C_1 is near zero and the predicted reduced Mooney stress is rather close to linear in $1/\lambda$ (see Figures 3b and 4). In this case, for low cross-link densities we find $C_2 \gg C_1$, contrary to the explicit predictions of the Rubinstein–Panyukov models,^{12,16} Wager’s MSFM,^{9,10} and the ME double tube model.¹⁴ As we have seen, all tube models with the exception of the ME and EV models are represented well by the Heinrich–Straube model with negative tube scaling exponents.

The RP, MSFM, and ME models, as well as the EV model with low slippage parameter $\eta < 0.1$, appear applicable to microstructurally very homogeneous, mostly sulfur-vulcanized rubbers. In this case, $C_2 \leq C_1$ and a constant or even decreasing C_2 with increasing cross-link density have been observed.^{27,38,59} A low slippage parameter $\eta = 0.08$ was found to fairly well

describe biaxial stress–strain data²⁰ of end-linked model networks of PDMS.

Systems comparable to ours, for which a rather significantly increasing C_2 and $C_2 > C_1$ with cross-linking was reported, are thiuram-vulcanized NR,^{43,62} sulfur-vulcanized styrene–butadiene rubber (SBR) with a special accelerator system,⁵⁹ and sulfur-cured NR made of short precursor chains.²⁷ Note that not all the cited results are strictly comparable, as the way in which the MR plots were evaluated differ. Rather large C_2 values have also been found for sulfur-vulcanized latex preparations of NR⁷⁶ and for peroxide-cross-linked poly(ethylene) networks.^{53,77} Analogous results and their interpretation based upon the EV model with larger slippage parameters ($\eta > 0.4$) have been reported for peroxide-cured *cis*-IR⁶³ and radiation-cross-linked polyethylene networks.⁶⁴

With the exception of the homogeneous sulfur-based NR systems of Veyres et al.³⁸ with small C_2 , none of the mentioned samples has been probed by NMR with regards to the sample inhomogeneity. We only know from our previous work that peroxide-cross-linked NR is characterized by extensive cross-linking inhomogeneities and a rather large fraction of short-chain defects.³³ For such samples, Klüppel has reported only slightly increasing C_2 values that are initially larger than C_1 at low cross-linking. In this limit, and generally in more-defect-rich rubbers, apparent tube scaling exponents appear to be positive (or slippage parameters tend to be larger than 0.1), which means that the apparent C_2 is indeed a good measure of the entanglement contributions. This applies to the systems studied herein, for which we can conclude that the x-linking inhomogeneity of the matrix and the amount of large, possibly branched defect structures are as relevant as the short-chain defect content.

E. Conclusions. In summary, we have presented a combined analysis of a series of lowly cross-linked latex-based natural rubber by two different macroscopic techniques (uniaxial stress–strain and equilibrium swelling) and a microscopic technique, i.e., low-field NMR as applied to bulk and swollen samples. NMR on swollen samples, when suitably back-extrapolated to the dry state, referred to as “phantom reference network”, reveals a cross-link-only contribution that is in perfect linear agreement with swelling results. The difference to the bulk NMR result reflects the entanglement contribution, which in turn was found to be proportional to the C_2 term from Mooney–Rivlin analysis. The consistency of these findings suggests that the samples can be described by the Heinrich–Straube tube theory with positive scaling exponent $\nu > 0.3$ or the Edwards–Vilgis slip-link model with slippage parameter $\eta > 1$.

We can conclude that the system studied herein, despite its comparably low short-chain defect fraction characteristic for conventionally peroxide-cured NR, is dominated by entanglement constraints whose detailed influence on the mechanical behavior bears a relation to cross-linking inhomogeneities and defect structures with high molecular weight. The former are reflected in the inhomogeneous distribution of residual dipole–dipole couplings measured by NMR in the bulk, while the latter are revealed through their fast relaxation in swollen samples and their correspondingly long transverse relaxation times as seen by NMR (note the inverse relation). However, such large defect structures appear to contribute to the long-time elastic properties of bulk samples probed in the tensile tests, where they suffer a significant slowdown. The role of such possibly very slow or even topologically frustrated relaxation of these components will be the focus of future studies.

More refined discussions should possibly also include the assessment of the actual fraction of trapped entanglements, which was here simply treated as additive to the apparent chemical cross-link density.

We expect our experimental strategy, in particular the use of NMR in assessing the sample (in)homogeneity and defect content, and the phantom reference network based separation of cross-link and entanglement contributions, to be of much use in understanding the large qualitative differences in the mechanical behavior of rubbers prepared by different protocols. In addition, a wider-scale application of biaxial stress-strain experiments is desirable, as this is the only strategy which allows for a truly objective distinction between different elasticity models.^{18–20} Obviously, a final and universal elucidation of the molecular underpinnings of entanglement effects on rubber elasticity must comprise a detailed assessment of the network inhomogeneity and defects.

■ ASSOCIATED CONTENT

Supporting Information

Experimental details. This material is available free of charge via the Internet at <http://pubs.acs.org>.

■ AUTHOR INFORMATION

Corresponding Author

*E-mail: kay.saalwaechter@physik.uni-halle.de (K.S.).

Notes

The authors declare no competing financial interest.

Biographies



Sandra Schlägl received her Diploma in Technical Chemistry from the University of Technology in Graz, Austria, in 2006. She then joined the Polymer Competence Center Leoben (PCCL) GmbH in Austria, where she has been working on the chemistry and technology of photochemical cross-linking methods for diene rubber materials. In 2008, she received her PhD in Polymer Chemistry from the University of Technology in Graz. Currently, she works as a senior doctoral researcher at PCCL in cooperation with leading polymer and elastomer companies in Austria. In her present research work she focuses on new cross-linking and surface functionalization strategies for smart elastomer and composite materials.



Marie-Luise Trutschel has been a PhD student since 2011. She studied Medical Physics at the Martin-Luther-University Halle-Wittenberg (Halle, Germany) and received her Diploma in 2011. Since 2009 she has been working with Prof. Kay Saalwächter on the study of structure and dynamics in polymer melts, blends, and elastomers by multiple-quantum NMR experiments and complementary techniques.



Walter Chassé received his Diploma (2007) and Ph.D. (2013) degrees in physics from the Martin-Luther-University Halle-Wittenberg (Halle, Germany). He worked in the group of Prof. Kay Saalwächter, investigating structure, formation, and thermodynamic properties of polymer networks by various NMR techniques and swelling experiments. In 2013, he moved to Radboud University Nijmegen, working as a postdoctoral fellow in the lab of Prof. Arno Kentgens. He is involved in a DPI project developing high-field NMR methodology for the investigation of semicrystalline polymers and the influence of stress on the phase composition.



Gisbert Riess received his PhD in polymer chemistry at the University of Bayreuth under the supervision of Prof. Oskar Nuyken (Macro-

molecular Chemistry) in 1993. After a postdoc period at the University of Bayreuth and the Technical University of Munich, in 2001 he moved to the chair of Chemistry of Polymeric Materials at the Montanuniversität Leoben. Since 2007 he is working as an assistant professor at the chair of Chemistry of Polymeric Materials in Leoben and since 2013 as a key researcher at the Polymer Competence Center Leoben (PCCL). His areas of expertise cover the chemical modification of filler surfaces as well as thermoplastic silicone elastomers and barrier layers.



Kay Saalwächter received his Diploma in Chemistry in 1997 at the Institute of Macromolecular Chemistry (University of Freiburg, Germany). In 2000, he finished his Doctorate at the Max-Planck Institute for Polymer Research and the University of Mainz, Germany, followed by his Habilitation in 2004 at the Institute of Macromolecular Chemistry (University of Freiburg, Germany). Since 2005 he has been holding a Professorship of Experimental Physics at the Martin-Luther-University Halle-Wittenberg (Halle, Germany). He had his first contact with polymer solid-state NMR on an exchange visit to the University of Massachusetts (Amherst) working with Klaus Schmidt-Rohr; ever since his continuing research interest has been the development and application of NMR techniques to the study of structure and dynamics in polymeric, liquid-crystalline, biological, and other “soft” materials, which have been published in about 100 papers.

ACKNOWLEDGMENTS

This work benefited from many intense discussions with a number of colleagues. We thank in particular Manfred Wagner, Manfred Klüppel, Gert Heinrich, Ekkehard Straube, Jörg Tiller, and an anonymous reviewer for their invaluable input. Partial funding was provided by the Deutsche Forschungsgemeinschaft (DFG SA982/4-2).

REFERENCES

- (1) Flory, P. J.; Rehner, J., Jr. Statistical Mechanics of Cross-Linked Polymer Networks I. Rubberlike Elasticity. *J. Chem. Phys.* **1943**, *11*, 512–520.
- (2) James, H. M.; Guth, E. Theory of the Elastic Properties of Rubber. *J. Chem. Phys.* **1943**, *11*, 455–481.
- (3) Ronca, G.; Allegra, G. An Approach to Rubber Elasticity with Internal Constraints. *J. Chem. Phys.* **1975**, *63*, 4990–4997.
- (4) Marrucci, G. Rubber Elasticity Theory. A Network of Entangled Chains. *Macromolecules* **1981**, *14*, 434–442.
- (5) Ball, R. C.; Doi, M.; Edwards, S. F.; Warner, M. Elasticity of Entangled Networks. *Polymer* **1981**, *22*, 1010–1018.
- (6) Edwards, S. F.; Vilgis, T. The Effect of Entanglements in Rubber Elasticity. *Polymer* **1986**, *27*, 483–492.
- (7) Heinrich, G.; Straube, E.; Helmis, G. Rubber Elasticity of Polymer Networks - Theories. *Adv. Polym. Sci.* **1988**, *85*, 33–87.
- (8) Edwards, S. F.; Vilgis, T. A. The Tube Model of Rubber Elasticity. *Rep. Prog. Phys.* **1988**, *51*, 243–297.
- (9) Wagner, M. H.; Schaeffer, J. Rubbers and Polymer Melts: Universal Aspects of Nonlinear Stress-Strain Relations. *J. Rheol.* **1993**, *37*, 643–661.
- (10) Wagner, M. H. The Origin of the C_2 Term in Rubber Elasticity. *J. Rheol.* **1994**, *38*, 655–679.
- (11) Heinrich, G.; Kaliske, M. Theoretical and Numerical Formulation of a Molecular Based Constitutive Tube-Model of Rubber Elasticity. *Comp. Theor. Polym. Sci.* **1997**, *7*, 227–241.
- (12) Rubinstein, M.; Panyukov, S. Nanaffine Deformation and Elasticity of Polymer Networks. *Macromolecules* **1997**, *30*, 8036–8044.
- (13) Klüppel, M.; Schramm, J. A Generalized Tube Model of Rubber Elasticity and Stress Softening of Filler Reinforced Elastomer Systems. *Macromol. Theory Simul.* **2000**, *9*, 742–754.
- (14) Mergell, B.; Everaers, R. Tube Models for Rubber–Elastic Systems. *Macromolecules* **2001**, *34*, 5675–5686.
- (15) Heinrich, G.; Klüppel, M.; Vilgis, T. A. Reinforcement of Elastomers. *Curr. Opin. Solid State Mater. Sci.* **2002**, *6*, 195–203.
- (16) Rubinstein, M.; Panyukov, S. Elasticity of Polymer Networks. *Macromolecules* **2002**, *35*, 6670–6686.
- (17) Gottlieb, M.; Gaylord, R. J. Experimental Tests of Entanglement Models of Rubber Elasticity. 1. Uniaxial Extension. *Polymer* **1983**, *24*, 1644–1646.
- (18) Gottlieb, M.; Gaylord, R. J. Experimental Tests of Entanglement Models of Rubber Elasticity. 3. Biaxial Deformations. *Macromolecules* **1987**, *20*, 130–138.
- (19) Kawamura, T.; Urayama, K.; Kohjiya, S. Multiaxial Deformations of End-Linked Poly(dimethylsiloxane) Networks. 1. Phenomenological Approach to Strain Energy Density Function. *Macromolecules* **2001**, *34*, 8252–8260.
- (20) Urayama, K.; Kawamura, T.; Kohjiya, S. Multiaxial Deformations of End-linked Poly(dimethylsiloxane) Networks. 2. Experimental Tests of Molecular Entanglement Models of Rubber Elasticity. *Macromolecules* **2001**, *34*, 8261–8269.
- (21) Bitoh, Y.; Akuzawa, N.; Urayama, K.; Takigawa, T. Strain Energy Function of Swollen Polybutadiene Elastomers Studied by General Biaxial Strain Testing. *J. Polym. Sci., Part B: Polym. Phys.* **2010**, *48*, 721–728.
- (22) Yohsuke, B.; Urayama, K.; Takigawa, T.; Ito, K. Biaxial Strain Testing of Extremely Soft Polymer Gels. *Soft Matter* **2011**, *7*, 2632–2638.
- (23) Straube, E.; Urban, V.; Pyckhout-Hintzen, W.; Richter, D.; Glinka, C. J. Small-Angle Neutron Scattering Investigation of Topological Constraints and Tube Deformation in Networks. *Phys. Rev. Lett.* **1995**, *74*, 4464–4467.
- (24) Pyckhout-Hintzen, W.; Westermann, S.; Wischnewski, A.; Monkenbusch, M.; Richter, D.; Straube, E.; Farago, B.; Lindner, P. Direct Observation of Nonaffine Tube Deformation in Strained Polymer Networks. *Phys. Rev. Lett.* **2013**, *110*, 196002.
- (25) Read, D. J.; McLeish, T. C. B. “Lozenge” Contour Plots in Scattering from Polymer Networks. *Phys. Rev. Lett.* **1997**, *87*, 87–90.
- (26) Litvinov, V. M.; Barendswaard, W.; van Duin, M. The Density of Chemical Crosslinks and Chain Entanglements in Unfilled EPDM Vulcanizates As Studied with Low Resolution, Solid State H-1 NMR. *Rubber Chem. Technol.* **1998**, *71*, 468–518.
- (27) Klüppel, M.; Menge, H.; Schmidt, H.; Schneider, H.; Schuster, R. H. Influence of Preparation Conditions on Network Parameters of Sulfur-Cured Natural Rubber. *Macromolecules* **2001**, *34*, 8107–8116.
- (28) Saalwächter, K.; Herrero, B.; López-Manchado, M. A. Chain Order and Crosslink Density of Elastomers As Investigated by Proton Multiple-Quantum NMR. *Macromolecules* **2005**, *38*, 9650–9660.
- (29) Saalwächter, K. Proton Multiple-Quantum NMR for the Study of Chain Dynamics and Structural Constraints in Polymeric Soft Materials. *Prog. NMR Spectrosc.* **2007**, *51*, 1–35.
- (30) Giuliani, J. R.; Gjersing, E. L.; Chinn, S. C.; Jones, T. V.; Wilson, T. S.; Alviso, C. T.; Pearson, M. A.; Herberg, J. L.; Maxwell, R. S. Thermal Degradation in a Trimodal Poly(dimethylsiloxane) Network Studied by ¹H Multiple Quantum NMR. *J. Phys. Chem. B* **2007**, *111*, 12977–12984.
- (31) Orza, R.; Magusin, P. C. M. M.; Litvinov, V. M.; van Duin, M.; Michels, M. A. J. Solid-State ¹H NMR Study on Chemical Cross-Links,

- Chain Entanglements, and Network Heterogeneity in Peroxide-Cured EPDM Rubbers. *Macromolecules* **2007**, *40*, 8999–9008.
- (32) Valentín, J. L.; Carretero-González, J.; Mora-Barrantes, I.; Chassé, W.; Saalwächter, K. Uncertainties in the Determination of Cross-Link Density by Equilibrium Swelling Experiments in Natural Rubber. *Macromolecules* **2008**, *41*, 4717–4729.
- (33) Valentín, J. L.; Posadas, P.; Fernández-Torres, A.; Malmierca, M. A.; González, L.; Chassé, W.; Saalwächter, K. Inhomogeneities and Chain Dynamics in Diene Rubbers Vulcanized with Different Cure Systems. *Macromolecules* **2010**, *43*, 4210–4222.
- (34) Che, J.; Toki, S.; Valentín, J. L.; Brasero, J.; Nimpairoon, A.; Rong, L.; Hsiao, B. S. Chain Dynamics and Strain-Induced Crystallization of Pre- and Postvulcanized Natural Rubber Latex Using Proton Multiple Quantum NMR and Uniaxial Deformation by *in Situ* Synchrotron X-ray Diffraction. *Macromolecules* **2012**, *45*, 6491–6503.
- (35) Saalwächter, K. Microstructure and Dynamics of Elastomers As Studied by Advanced Low-Resolution NMR Methods. *Rubber Chem. Technol.* **2012**, *85*, 350–386.
- (36) Chassé, W.; Lang, M.; Sommer, J.-U.; Saalwächter, K. Cross-Link Density Estimation of PDMS Networks with Precise Consideration of Networks Defects. *Macromolecules* **2012**, *45*, 899–912.
- (37) Chassé, W.; Saalwächter, K.; Sommer, J.-U. Thermodynamics of Swollen Networks As Reflected in Segmental Orientation Correlations. *Macromolecules* **2012**, *45*, 5513–5523.
- (38) Vieyres, A.; Pérez-Aparicio, R.; Albouy, P.-A.; Sanseau, O.; Saalwächter, K.; Long, D. R.; Sotta, P. Sulfur-Cured Natural Rubber Elastomer Networks: Correlating Crosslink Density, Chain Orientation and Mechanical Response by Combined Techniques. *Macromolecules* **2013**, *46*, 889–899.
- (39) Chassé, W.; Schlägl, S.; Riess, G.; Saalwächter, K. Inhomogeneities and Local Chain Stretching in Partially Swollen Networks. *Soft Matter* **2013**, *9*, 6943–6954.
- (40) Pérez-Aparicio, R.; Schiewek, M.; Valentín, J. L.; Schneider, H.; Long, D. R.; Saphiannikova, M.; Sotta, P.; Saalwächter, K.; Ott, M. Local Chain Deformation and Overstrain in Reinforced Elastomers: An NMR Study. *Macromolecules* **2013**, *46*, 5549–5560.
- (41) Callaghan, P. T.; Samulski, E. T. Biaxial Deformation of a Polymer Network Measured via Deuteron Quadrupolar Interactions. *Macromolecules* **2003**, *36*, 724–735.
- (42) Mooney, M. A Theory of Large Elastic Deformation. *J. Appl. Phys.* **1940**, *11*, 582–592.
- (43) Klüppel, M. Trapped Entanglements in Polymer Networks and Their Influence on the Stress-Strain Behavior up to Large Extensions. *Prog. Colloid Polym. Sci.* **1992**, *90*, 137–143.
- (44) Flory, P. J.; Rehner, J., Jr. Statistical Mechanics of Cross-Linked Polymer Networks II. Swelling. *J. Chem. Phys.* **1943**, *11*, 521–526.
- (45) Saalwächter, K.; Chassé, W.; Sommer, J.-U. Structure and Swelling of Polymer Networks: Insights from NMR. *Soft Matter* **2012**, *9*, 6587–6593.
- (46) McKenna, G. B.; Flynn, K. M.; Chen, Y. Experiments on the Elasticity of Dry and Swollen Networks: Implications for the Frenkel-Flory-Rehner Hypothesis. *Macromolecules* **1989**, *22*, 4507–4512.
- (47) McKenna, G. B.; Flynn, K. M.; Chen, Y. Swelling in Crosslinked Natural Rubber: Experimental Evidence of the Crosslink Density Dependence of χ . *Polymer* **1990**, *31*, 1937–1945.
- (48) Horkay, F.; McKenna, G. B.; Deschamps, P.; Geissler, E. Macroscopic and Microscopic Thermodynamic Observations in Swollen Poly(vinyl acetate) Networks. *Macromolecules* **1991**, *24*, 2896–2902.
- (49) McKenna, G. B.; Horkay, F. Effects of Crosslinks on the Thermodynamics of Poly(vinyl alcohol) Hydrogels. *Polymer* **1994**, *35*, 5737–5742.
- (50) Horta, A.; Pastoriza, M. A. The Interaction Parameter of Crosslinked Networks and Star Polymers. *Eur. Polym. J.* **2005**, *41*, 2793–2802.
- (51) Patel, S. K.; Malone, S.; Cohen, C.; Gillmor, J. R.; Colby, R. H. Elastic Modulus and Equilibrium Swelling of Poly(dimethylsiloxane) Networks. *Macromolecules* **1992**, *25*, 5241–5251.
- (52) Treloar, L. R. G. *The Physics of Rubber Elasticity*; Oxford University Press: Oxford, 1975.
- (53) Kolesov, I. S.; Radusch, H. J. Multiple Shape-Memory Behavior and Thermal-Mechanical Properties of Peroxide Cross-Linked Blends of Linear and Short-Chain Branched Polyethylenes. *eXPRESS Polym. Lett.* **2008**, *2*, 461–473.
- (54) Akagi, Y.; Gong, J. P.; Chung, U.-L.; Sakai, T. Transition between Phantom and Affine Network Model Observed in Polymer Gels with Controlled Network Structure. *Macromolecules* **2013**, *46*, 1035–1040.
- (55) Saalwächter, K. Artifacts in Transverse Proton NMR Relaxation Studies of Elastomers. *Macromolecules* **2005**, *38*, 1508–1512.
- (56) Saalwächter, K.; Kleinschmidt, F.; Sommer, J.-U. Swelling Heterogeneities in End-Linked Model Networks: A Combined Proton Multiple-Quantum NMR and Computer Simulation Study. *Macromolecules* **2004**, *37*, 8556–8568.
- (57) Sommer, J.-U.; Chassé, W.; Valentín, J. L.; Saalwächter, K. Effect of Excluded Volume on Segmental Orientation Correlations in Polymer Chains. *Phys. Rev. E* **2008**, *78*, 051803.
- (58) Chassé, W.; Valentín, J. L.; Genesky, G. D.; Cohen, C.; Saalwächter, K. Precise Dipolar Coupling Constant Distribution Analysis in Proton Multiple-Quantum NMR of Elastomers. *J. Chem. Phys.* **2011**, *134*, 044907.
- (59) Klüppel, M.; Heinrich, G. Network Structure and Mechanical Properties of Sulfur-Cured Rubbers. *Macromolecules* **1994**, *27*, 3596–3603.
- (60) Rubinstein, M.; Colby, R. H. *Polymer Physics*; Oxford University Press: New York, 2003.
- (61) Lang, M.; Sommer, J.-U. Analysis of Entanglement Length and Segmental Order Parameter in Polymer Networks. *Phys. Rev. Lett.* **2010**, *104*, 177801.
- (62) Klüppel, M. Network Structure and Mechanical Properties of Elastomers. Part 2. Influence of Strain-Induced Crystallization on Stress-Strain Data. *Kautsch. Gummi, Kunstst.* **1993**, *46*, 241–247.
- (63) Thirion, P.; Weil, T. Assessment of the Sliding Link Model of Chain Entanglement in Polymer Networks. *Polymer* **1984**, *25*, 609–614.
- (64) Brereton, M. G.; Klein, P. G. Analysis of the Rubber Elasticity of Polyethylene Networks Based on the Slip Link Model of S. F. Edwards *et al.* *Polymer* **1988**, *29*, 970–974.
- (65) Svaneborg, C.; Grest, G. S.; Everaers, R. Strain-Dependent Localization, Microscopic Deformations, and Macroscopic Normal Tensions in Model Polymer Networks. *Phys. Rev. Lett.* **2004**, *93*, 257801.
- (66) Saalwächter, K. Comment on “Chain Entanglements in Polyethylene Melts. Why Is It Studied Again?”. *Macromolecules* **2013**, *46*, 5090–5093.
- (67) Cohen-Addad, J. P.; Domard, M.; Lorentz, G.; Herz, J. Polymeric Gels. NMR Study of Elementary Chain Swelling. Effect of Trapped Topological Constraints. *J. Phys. (Paris)* **1984**, *45*, 575–586.
- (68) Schlägl, S.; Temel, A.; Schaller, R.; Holzner, A.; Kern, W. Prevulcanization of Natural Rubber Latex by UV Techniques: A Process towards Reducing Type IV Chemical Sensitivity of Latex Articles. *Rubber Chem. Technol.* **2012**, *83*, 3478–3486.
- (69) Schlägl, S.; Temel, A.; Schaller, R.; Holzner, A.; Kern, W. Characteristics of the Photochemical Prevulcanization in a Falling Film Photoreactor. *J. Appl. Polym. Sci.* **2012**, *124*, 3478–3486.
- (70) Abdel-Goad, M.; Pyckhout-Hintzen, W.; Kahle, S.; Allgaier, J.; Richter, D.; Fetters, L. J. Rheological Properties of 1,4-Polyisoprene over a Large Molecular Weight Range. *Macromolecules* **2004**, *37*, 8135–8144.
- (71) Fetters, L. J.; Lohse, D. J.; Colby, R. H. Chain dimensions and entanglement spacings. In Mark, J. E., Ed.; *Physical Properties of Polymers Handbook*; Springer: New York, 2007; Chapter 25, pp 447–454.
- (72) Sanders, J. F.; Ferry, J. D.; Valentine, R. H. Viscoelastic Properties of 1,2-Polybutadiene—Comparison with Natural Rubber and Other Elastomers. *J. Polym. Sci., Part A-2* **1968**, *6*, 967–980.
- (73) Macosko, C. W.; Miller, D. R. A New Derivation of Average Molecular Weights of Nonlinear Polymers. *Macromolecules* **1976**, *9*, 199–206.
- (74) Heuwers, B.; Beckel, A.; Krieger, A.; Katzenberg, F.; Tiller, J. C. Shape-Memory Natural Rubber: An Exceptional Material for Strain and Energy Storage. *Macromol. Chem. Phys.* **2013**, *214*, 912–923.

(75) Graf, R.; Heuer, A.; Spiess, H. W. Chain-Order Effects in Polymer Melts Probed by ^1H Double-Quantum NMR Spectroscopy. *Phys. Rev. Lett.* **1998**, *80*, 5738–5741.

(76) Winsunthorn, S.; Bonfils, F.; Pochat-Bohatier, C.; Bouyer, D.; Deratani, A.; Dupuy, C. Comparative Study of the Elasticity and Permeability of Vulcanized Films Made with Skim and Cream Natural Rubber Latex. *J. Appl. Polym. Sci.* **2008**, *108*, 960–968.

(77) Hoehler, R.; Raidt, T.; Rose, M.; Katzenberg, F.; Tiller, J. C. Recoverable Strain Storage Capacity of Shape Memory Polyethylene. *J. Polym. Sci., Part B: Polym. Phys.* **2013**, *51*, 1033–1040.